

Analyst

Accepted Manuscript



This is an *Accepted Manuscript*, which has been through the Royal Society of Chemistry peer review process and has been accepted for publication.

Accepted Manuscripts are published online shortly after acceptance, before technical editing, formatting and proof reading. Using this free service, authors can make their results available to the community, in citable form, before we publish the edited article. We will replace this *Accepted Manuscript* with the edited and formatted *Advance Article* as soon as it is available.

You can find more information about *Accepted Manuscripts* in the [Information for Authors](#).

Please note that technical editing may introduce minor changes to the text and/or graphics, which may alter content. The journal's standard [Terms & Conditions](#) and the [Ethical guidelines](#) still apply. In no event shall the Royal Society of Chemistry be held responsible for any errors or omissions in this *Accepted Manuscript* or any consequences arising from the use of any information it contains.

Cite this: DOI: 10.1039/c0xx00000x

www.rsc.org/xxxxxxx

ARTICLE TYPE

Measuring bacterial adaptation dynamics at the single-cell level using a microfluidic chemostat and time-lapse fluorescence microscopy

Zhicheng Long^a, Anne Olliver^b, Elisa Brambilla^b, Bianca Sclavi^b, Marco Cosentino Lagomarsino^{c,d} and Kevin D. Dorfman^{*a}

⁵ Received (in XXX, XXX) Xth XXXXXXXXX 20XX, Accepted Xth XXXXXXXXX 20XX

DOI: 10.1039/b000000x

We monitored the dynamics of cell dimensions and reporter GFP expression in individual *E. coli* cells growing in a microfluidic chemostat using time-lapse fluorescence microscopy. This combination of techniques allows us to study the dynamical responses of single bacterial cells to nutritional shift-down or shift-up for longer times and with more precision over the chemical environment than similar experiments performed on conventional agar pads. We observed two *E. coli* strains containing different promoter-reporter gene constructs and measured how both their cell dimensions and the GFP expression change after nutritional upshift and downshift. As expected, both strains have similar adaptation dynamics for cell size rearrangement. However, the strain with a ribosomal RNA promoter dependent reporter has a faster GFP production rate than the strain with a constitutive promoter reporter. As a result, the mean GFP concentration in the former strain changes rapidly with the nutritional shift, while that in the latter strain remains relatively stable. These findings characterize the present microfluidic chemostat as a versatile platform for measuring single-cell bacterial dynamics and physiological transitions.

Introduction

Bacteria can survive in very different environments. They sense and adapt to changes in their external environment by altering the expression of their genes to result in new physiological states¹⁻⁴. Although the development of various fluorescent proteins has enabled researchers to quantify the gene expression levels in bacterial cells⁵⁻⁷, it is still challenging to monitor with high resolution the gene expression dynamics in live cells in balanced growth for a long period of time, especially at the single cell level.

The most popular technique for measuring single-cell gene expression is flow cytometry^{6, 8-11}. Flow cytometry allows researchers to measure the abundance of fluorescent proteins and cell size at a rate of thousands cells per second. It thereby provides great accuracy for population average measurements and the distribution of gene activities in individual cells over time. However, flow cytometry has some important drawbacks, limiting its application in single-cell dynamics measurements. First, flow cytometry is expensive and requires specialized training. Second, it cannot provide time-lapse information from the same group of cells because the measured cells are discarded. Third, the bacteria samples usually need to be disaggregated, re-suspended in a buffer and fixed before being analyzed by flow cytometry. These sample preparation steps reduce the actual temporal resolution of this technique and limit its use in monitoring the dynamics of rapid cellular changes. Finally, flow cytometry cell sizing is based on the measurement of forward light scatter, which is not very precise for measuring the size of

sub-micron bacterial cells due to the nonlinear relationship between forward scattering and cell size¹². As a result, flow cytometry is not suitable to measure the dynamics of protein concentration in individual bacterial cells.

Another widely used method for monitoring the dynamics of fluorescent protein abundance and cell size is time-lapse microscopy¹³⁻¹⁷. While the limited field of view of a microscope prevents monitoring thousands of cells at a time, as in flow cytometry, microscopy allows one to monitor the dynamic behaviours of individual cells for a long time with good precision and high temporal resolution. Conventional time-lapse microscopy measurements of individual bacterial cells are performed on thin agar pads¹⁵. However, the agar-based platform has two major limitations for adaptation studies: (i) it is very challenging to quickly change the chemical environment on an agar pad due to the slow hindered diffusion of macromolecules in agar; and (ii) the observation time cannot be longer than 6 to 8 generations because the tightly packed growing cells form a multilayer colony and deplete the reagents and nutrients in the pad.

These limitations have motivated the development of microfluidic chemostats to grow and observe individual bacterial cells over many generations, along with control over the chemical conditions. Despite the various microfluidic designs appearing in the literature, these microchemostats share two common features: (i) The cells are trapped in microstructures with heights of $\sim 1 \mu\text{m}$ and can only grow into monolayer colonies; and (ii) continuous flow replenishes the nutrient supply and removes the excess cells and the side products of cellular metabolism, maintaining a

constant environment. The first type of bacteria microchemostat confines the bacterial cell in $\sim 1 \mu\text{m}$ -deep microchambers^{13, 18-23} and the cells grow two-dimensionally. While the chamber bottom is usually a thin glass coverslip, the materials of the chamber lid could be PDMS^{18-20, 23}, a semipermeable membrane¹³ or a soft gel^{21, 22} like agar and polyacrylamide. For example, Boulineau *et al.* measured the *lac* expression and the growth dynamics of individual cells during diauxic shift by growing the *E. coli* cells in a shallow chamber formed between a polyacrylamide membrane and a coverslip²². Wakamoto *et al.* grew *Mycobacterium smegmatis* between a coverslip and a semipermeable membrane under PDMS flow channels and studied the dynamic persistence of single cells under isoniazid exposure¹³. More recently, Nobs *et al.* reported a PDMS-based microfluidic device consisting of 120 microchemostat growth chambers which allows them to grow *S. pombe* for several days and quantitate over 100000 divisions in a single experiment²³. The microcolony in these chamber-based microchemostat is randomly packed, as is the case on agar. In contrast, the second type of microchemostat confines the cells in narrow microchannels and forces the cells to grow in lines²⁴⁻²⁷. The population in these one-dimensional microcolonies is controlled by the channel length, typically from single bacterium²⁷ to several cells²⁴⁻²⁶. This oriented small population simplifies the image processing and lineage identification.

In our previous work²⁴, we developed a microfluidic microchemostat that allowed us to immobilize and grow thousands of *E. coli* cells chemostatically for over 50 generations. It consists of 600 narrow trapping/growth channels connected to a pair of big feeding channels on both ends. The open-end channel design leads the present microchemostat to faster loading of bacterial cells, easier nutrients delivery and lower filamentation rate than the dead-end mother machine²⁵. It also allows us to quickly change the growth media during the measurement, which is very challenging in agar-based microchemostats^{21, 22, 26}. We demonstrated its capability in measuring single-cell dynamics like loci tracking^{24, 28, 29} and, at the proof-of-principle level, GFP expression dynamics during media change²⁴. In this work, we present the application of our microchemostat for quantifying the dynamics of bacterial adaptive responses to nutritional shifts, going well beyond the proof-of-principle experiment in our earlier publication²⁴. We constructed two *E. coli* strains with different GFP reporter constructs, one of which is expressed in a constitutive fashion and the other of which responds to changes in the DNA's supercoiling density and cellular metabolism. We then monitored the dynamics of the change in cellular dimensions and GFP expression before and after the growth medium change with high temporal and spatial resolution.

Experimental

Bacterial strains and growth conditions

The two bacterial strains used in these experiments contain either the P1 or P5 promoters controlling the expression of GFP. The promoter construct, GFP gene and the gene coding for kanamycin resistance were inserted in the chromosome of *E. coli* BW25113 in the intragenic region between the *aidB* and *yj1N* genes (at 4,414,000), following the protocol by Datsenko and Wanner³⁰. P5

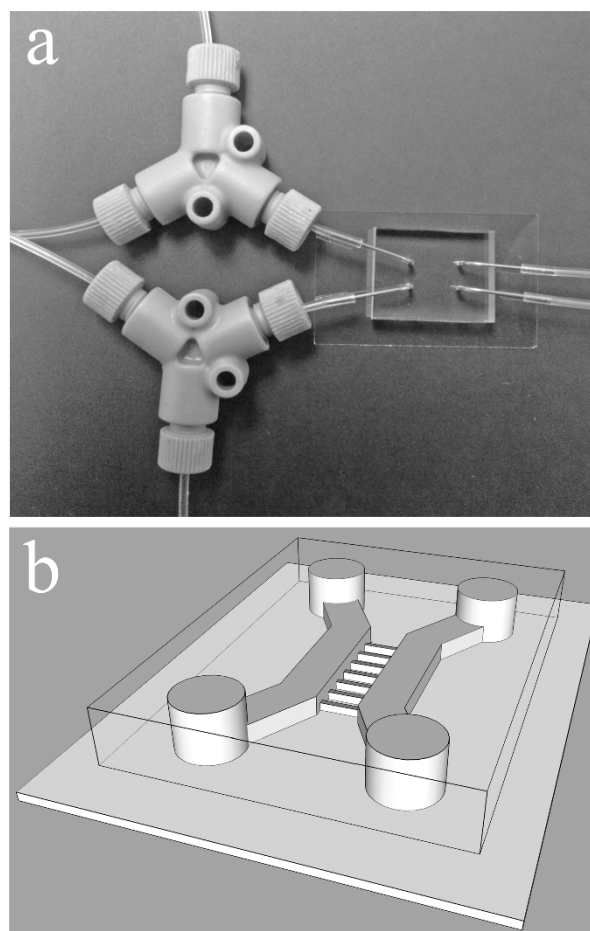


Fig. 1 The PDMS-based microfluidic chemostat. (a) Photo of the microchemostat, connection tubes and the PEEK Y connector. (b) Schematic layout of the microchannels. The microchemostat contains 600 shallow and narrow growth channels, which are about $20 \mu\text{m}$ long, $0.8 \mu\text{m}$ wide and $1.1 \mu\text{m}$ deep. The two feeding channels are $50 \mu\text{m}$ wide and $\sim 20 \mu\text{m}$ deep.

is an 84 base pair early promoter from the T5 phage genome with the sequence ACAACATCTAAGAGAAAAATTATA-TTGACATCTGCCCTTGAATAAGCTATAATAGTAGTCTT-AGTTAGAGAAGGAGGGTATAAT. It is considered a strong, constitutive promoter; the bolded TTGACA and TATAAT sequences, spaced exactly 17 base pairs apart, are consensus for both -35 and -10 regions that are recognized by the main *E. coli* RNA polymerase. As a result, the activity of P5 should increase with the amount of RNA polymerase available in the cell. P1 stands for the *rrnBP1* promoter. It is a well studied, 77 base pair ribosomal RNA promoter with the sequence TTGCGCGGTCA-GAAAATTATTTTAAATTTCTCTTGTTCAGGCCGGAATA-ACTCCCTATAATGCGCCACCACTGACA. This promoter has a GC-rich discriminator region at the start site of transcription (underlined) that renders it a reporter of the change in negative supercoiling, while it also has the -35 and -10 consensus sequences we saw in P5 that are recognized by RNA polymerase. This is a short version of the wild type *rrnBP1* promoter that lacks the upstream binding sites for Fis protein. The activity of P1 is expected to increase when negative supercoiling increases while also responding to the amount of RNA polymerase in the cell. This promoter is also a reporter for change in the

concentration of guanosine pentaphosphate (ppGpp), and its activity should increase when the amount of ppGpp in the cell decreases³¹.

The *E. coli* cells were first grown overnight at 37°C in Luria Broth (LB) medium with 50 µg/mL kanamycin. Then the overnight cultures were diluted 1000 fold into M9 minimal media supplemented with 0.2% casamino acids (CAA) and 50 µg/mL kanamycin and were grown to mid-log phase before being introduced into the microchemostat.

10 Growing *E. coli* cells in the microfluidic chemostat

The fabrication and operation of our microchemostat has been described in our previous paper²⁴. Briefly, bacterial cells were trapped in an array of 20(L) × 0.8(W) × 1.1(D) -µm growth channels connected to a pair of deep and wide feeding channels, as illustrated in figure 1. When a slow flow of fresh growth media is maintained in both feeding channels, the bacterial cells trapped in the narrow growth channels keep growing and dividing in lines and the excess cells are washed away by the flow. Practically, the flow rates in the two feeding channels are kept at 1.2 µL/min and 0.6 µL/min, respectively. The concomitant pressure difference between feeding channels thus leads to weak flow across each of the growth channels, which ensures sufficient nutrient delivery to the trapped growing cells while keeping the flow rate low enough to avoid pushing the cells out of the growth channels or distressing them with a high shear rate. The microchemostat was placed in a homemade, heated aluminium holder and the temperature was maintained at 30°C for all the microdevice experiments in this study.

31 Changing growth media

Two PEEK Y connectors (Upchurch, P-512) were used for changing the growth media in the microchemostat, as seen in figure 1a. Each Y connector connects to two syringes filled with different growth media. The dead volume from the joint spot to the needle tip is ~5 µL. We typically maintain the same flow rates at 1.2 µL/min in both feeding channels during the media change to prevent the formation of concentration gradients across the growth channels; as a result, it typically took 4-6 minutes to completely replace the media inside all growth channels after the syringes were changed. When the two growth media have different fluorescence background intensities, the actual time point of the media shift can be observed from the time-lapse movie. Once the media in the channels has been changed, the flow rates in the two feeding channels were set back to 1.2 µL/min and 0.6 µL/min, respectively.

45 Time-lapse cell imaging

Imaging experiments were performed on an automated and inverted microscope (Leica DMI-4000B) equipped with a Photometrics CoolSnap EZ CCD camera and a motorized stage (Prior Scientific). An external Leica EL6000 light source was used to excite the fluorescence. The microscope, the camera and the xy stage were controlled with Micro-manager software³². Time-lapse movies were recorded every four minutes for six fields of view. Autofocus was triggered at every time point on the phase contrast channel through the embedded duo [simple autofocus and JAF (H&P)] autofocus module. To minimize photo bleaching, the pixel binning of the camera was set to 2 and the

fluorescence shutter opened only for the duration of the exposure time (typically 100ms).

Flow cytometry

Overnight cultures were obtained by inoculating a single colony into M9 minimal medium supplemented with 0.2% CAA and Kanamycin 50 µg/ml, and by incubating them at 37°C shaking. In the morning, cultures were diluted 200-fold into fresh M9 medium with 0.2% CAA, and grown to mid-log phase. Cultures were diluted again 10 fold in the same medium, in order to extend the exponential phase. After 2 hours, each culture was split in two, cells were centrifuged for 5 minutes at 3500 rpm at room temperature, and then resuspended either in M9 medium with 0.2% CAA, or in LB. Samples were harvested every ten minutes, centrifuged for 5 minutes at 4°C at 3500 rpm, washed with PBS buffer, fixed for 30 minutes at room temperature with 2% Formaldehyde solution (Sigma) and washed three times with PBS. The samples were then measured on a FACS Calibur flow cytometer (BD Biosciences) with a 488 nm laser, using the software BD CellQuest™ Pro. All instrument parameters were logarithmically amplified, with the following settings: FSC E01, SSC 368V, FL1 750V. Individual FSC, SSC and FL1 histograms were checked to be sure that the bell-shaped populations are not cut off on the display. An event rate of <1000 events per second was maintained in order to minimize the chance of coincidence and to improve population resolution. In the FSC versus SSC plot a live gate R1 was set around the bacterial population and a total of 20,000 events inside the gate were measured.

Data analysis

Fluorescence images were segmented and measured with the open-source software 'CellProfiler'³³. Because the captured images from the CCD camera are 12-bit but saved in 16-bit format, we first rescale and normalize the image intensity to the 12-bit range. We then applied a lenient threshold (method 'Background global') to identify the small regions covered by cells. The cells in the feeding channels are excluded automatically at this step so that only the cells inside the growth channels are analysed. After removing the background area, we apply a local threshold (two classes 'Otsu PerObject' method) to each sub-region identified upstream. By carefully selecting an appropriate threshold correction factor and the size of the smoothing filter, we are able to determine the contour of individual bacterial cells and perform the measurements of cell sizes and fluorescence intensity in each image frame.

The measurement data were processed with Origin 8.6 (OriginLab). Any defocused data points, which result from instabilities in the software autofocus in Micromanager, are removed by combination of data filtering/smoothing and frame-by-frame movie examination. We first apply a 40-points median filter to the time-series plot of the mean pixel intensity of cells in each image frame. The data points below the smooth curve are attributed to the defocused image frames and all the measurements from those frames will be masked in subsequent analysis.

110 Results and discussion

Image segmentation and data analysis

Cite this: DOI: 10.1039/c0xx00000x

www.rsc.org/xxxxxx

ARTICLE TYPE

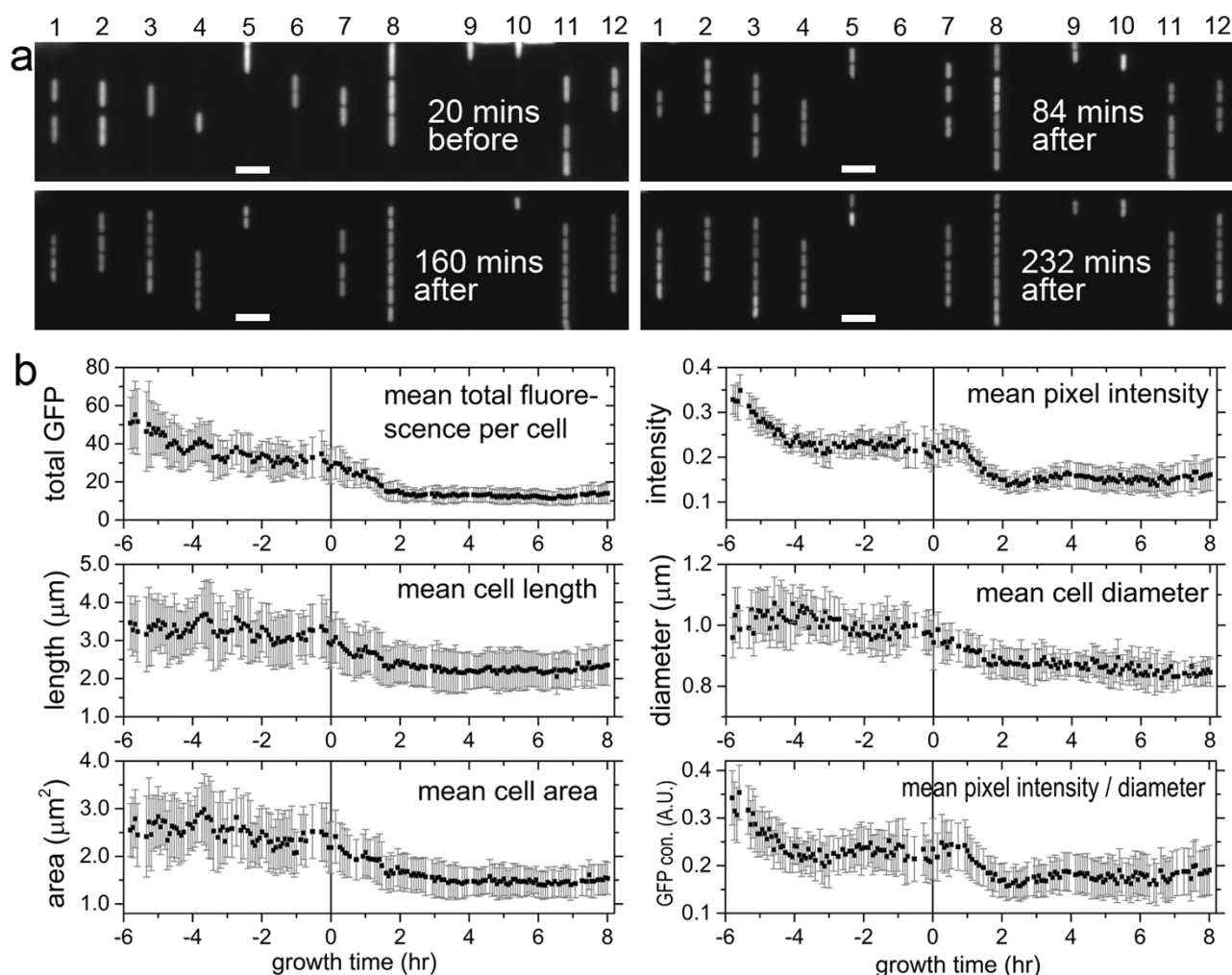


Fig. 2 Dynamic responses of *E. coli* cells to nutritional downshift. (a) Image frames extracted from movie S2 show the fluorescent cells, carrying the *rmBP1* promoter-GFP construct, altering their cellular dimensions and GFP expression during the nutritional downshift. The images are set with the same display range (max/min intensity and contrast) and the scale bar corresponds to 5 μm. The cells in the 5th, 9th and 10th growth channels in this particular experiment were excluded in our analysis because the mini-colonies in these channels were unstable. (b) Time-series plots of the population-averaged value (black squares) for various measurements. The standard deviations (shaded bars) represent the population heterogeneity in each frame. The defocused data points have been removed and the media shift time point is set as zero. The cells first grew in LB media for ~6 hours, then in M9 media with 0.2% CAA for ~8 hours. Both media contained 50 μg/mL kanamycin. The growth temperature was maintained at 30 °C.

A typical time-lapse movie obtained in our experiments is shown in movie S1. To monitor the dynamics of cell size and the expression of the GFP reporter, we need first to segment the individual cells from the background in each image frame. Although a number of commercial and open-source software packages have been developed to analyse microscopy images, image segmentation remains a central challenge in image analysis^{14,34}. In the gray-scale fluorescence image obtained in our experiments, the edges of the cells are smeared even in well-focused images, as seen in figure S1. The intensity profile in the direction of the cell width implies that the determination of the cell contour is not straightforward. Moreover, the background in

the images obtained on the microchemostat is non-uniform. The background intensities in the channel-free region are different from those in the feeding channels and in the unoccupied growth channels. It is difficult to separate the fluorescent cells with various intensities from such a non-uniform background using a global thresholding. Instead, a local thresholding method was used in this work. We built a processing pipeline containing two consecutive objects identification modules in the open-source software 'CellProfiler'³³. The first module uses a lenient threshold filter to remove most of the background area and to divide original image into tens of isolated sub-regions containing one or a few cells. The second module calculates different

1 thresholds (Otsu method) for each identified cell region,
2 determines the cell edges and distinguishes clumped cells. This
3 two-step local thresholding method allows us to find the
4 corresponding contour of most cells, as shown in figure S2. We
5 also found that a few clumped or elongated cells were not
6 correctly segmented. After determining the contours of cells, we
7 were able to perform a series of measurements of each identified
8 cell, including cell area, cell length, cell width and fluorescence
9 intensity within the cells.

10 Because the software-based autofocus we used for image
11 acquisition is based on a control algorithm using the image as the
12 input, rather than a hardware-based autofocusing, we observed
13 that some image frames display a blurry view of cells due to
14 imprecise focusing. Given the long duration of the experiment
15 and the number of fields of view, it is impractical to manually
16 focus the microscope. As shown in figure S2, the cell area
17 measured from defocused images is larger than the one from a
18 well-focused image, while the mean pixel intensity of the cells is
19 lower. Moreover, these defocused images are not widely
20 separated in time from the previous (focused) image in the stack,
21 so it is thus highly unlikely that the change between the two
22 images is due to biological activity. The significantly defocused
23 image frames are excluded in our analysis. To provide a
24 quantitative criterion, we apply a 40-points median filter to the
25 time-series plot of the population-averaged mean pixel intensity
26 of cells in each image frame. Figure S3a shows a typical raw data
27 plot and the smooth curve from the median filter. By careful
28 visual examination of the movies, we found that the data points
29 below the smooth curve all correspond to obviously defocused
30 image frames. Consequently, these data points, as well as the
31 measurements of other cellular parameters from the same frames,
32 are not included in the subsequent analysis. Figure S3b shows
33 that most of the defocused frames also result in a higher
34 measurement of mean cell area, again as an image defocusing
35 artefact.

36 In some movies we also observed unstable microcolonies in a
37 few of the growth channels. Occasionally, the flow in these
38 channels became unstable. As a result, the cells inside were
39 pushed out or new cells were squeezed into the unoccupied
40 channels in the middle of the experiment. These break-in new
41 cells are usually brighter than the equilibrated, well-trapped cells
42 and sometimes have different cell sizes, since they have not yet
43 been photobleached by the periodic light illumination, which
44 affects the population average measurements. Thus, we mask
45 these channels in our analysis, for example Lane 9 in figure 2a.

46 **Dynamic cellular response of *E. coli* to nutritional change**

47 It is well known that bacterial populations change their cell
48 dimensions^{35, 36} and gene expression³⁷ in different balanced
49 growth conditions. However, the dynamics during the transient
50 response to a nutrient change is not as well understood, especially
51 at the single cell level. As demonstrated briefly in our previous
52 paper²⁴, the present microfluidic chemostat allows us to grow
53 bacterial cells chemostatically for many generations while
54 maintaining a steady, essentially non-aging population of cells. It
55 also allows us to quickly change the growth media without
56 interrupting the time-lapse imaging. These features make the
57 microchemostat an ideal platform for studying the adaptation
58 behaviour of individual bacterial cells during the several hours

that it takes for them to respond to a step change in their chemical
60 environment.

We grew the engineered *E. coli* strains in the microchemostat
and monitored the cell size and GFP expression every 4 minutes
from several field of views using time-lapse microscopy. To
ensure that the bacteria population was at a steady state before the
65 nutrient switch, we first grew the cells in an initial growth
medium for at least 6 hours while periodically measuring their
fluorescence. This initial period allows the bacteria to adapt to the
microchannel environment. During this period, we observed an
70 obvious photobleaching effect in every experiment; the
fluorescence intensity of the exposed cells drops quickly in the
first few hours and then reaches a steady state where the
bleaching and dilution rate are balanced by the GFP production
rate, as shown in figure 2 and figure S3. Importantly, the cell
75 areas and the growth rate seem to be constant in the initial growth
medium, even in the first few hours, which implies that the light
dosage is still in safe range and the photo-damage of cells is
negligible in our experiments.

In the present experiments, we made an improvement
compared to our previous approach²⁴ for the change of the growth
80 medium. With the aid of two Y connectors, the media in the
growth channels could be changed in a minute, which is fast
relative to biological responses, in particular changes in gene
expression. We studied the adaptive behaviour of the reporter
strains in both nutritional upshift (from M9 minimal media to LB
85 media) and downshift (LB to M9) experiments. Figure 2 shows
representative images of the growing cells and the measurements
of various cellular parameters in a downshift experiment (movie
S2). In the movie, it is clear that some lanes (e.g. #9) have cells
that enter and leave the growth channel in the middle of
90 experiment. These lanes were excluded from subsequent analysis.
We track the population-averaged value of different parameter
measurements for each image frame. The cells growing in
nutrient-rich medium are longer than those in minimal medium.
We observed that long cells at the ends of the growth channels
95 seem to have a higher probability of being washed away by the
flow in the feeding channels. This can explain why the population
size per image frame in LB media is smaller (20-50 cells) than
that in M9 minimal media (40-80 cells).

From the image analysis described above we obtained the
100 cellular dimensions of the area, length and width, as well as the
integrated intensity and the mean pixel intensity of each
fluorescent cell. Because the depth of field/focus of the 100 \times , 1.3
NA objective used in our imaging experiments is ~ 0.7 μm ,
roughly equal to the mean diameter of *E. coli* cells growing in
105 M9 media, we thus assume that the well-focused images obtained
in our experiments capture the fluorescence from all GFP
molecules in the cells. Consequently, the integrated or total
fluorescence intensities measured from a single bacterial cell,
 F_{total} , could be roughly described by the relationship

$$110 F_{\text{total}} = KVC \quad (1)$$

where K is a constant, V is the cell volume and C is the GFP
concentration. If we assume that the rod shaped *E. coli* cells are
perfect cylindrical cells, then we get

$$115 F_{\text{total}} = K\pi D^2 LC/4 \quad (2)$$

Here D is the cell diameter and L is the cell length. Since the
mean pixel intensity of a cell, F_{pixel} , can be written as

$$F_{\text{pixel}} = F_{\text{total}}/DL \quad (3)$$

Equation (2) can then be rearranged into

$$C = \frac{4}{K\pi} \frac{F_{\text{pixel}}}{D} \quad (4)$$

We could thus estimate the mean GFP concentration in the growing cells by dividing the mean pixel intensity of cells by the measured cell width (diameter).

Figure 2b shows that the *E. coli* cells respond to the nutritional downshift by shrinking both the cell length and the cell diameter, as observed by other researchers^{38, 39}. Meanwhile, the total amount of GFP per cell and the mean GFP concentration of cells also decrease in the downshift experiment. The decrease of GFP fluorescence occurs because the activity of the promoters depends on the growth rate of cells. In our microchemostat experiments at 30°C, the mean division times of the P1 strain in LB media and M9 media with 0.2% CAA are 47±2 minutes and 131±4 minutes, respectively. The faster growth rate in LB media leads to higher promoter activity and increased gene copy number and thus higher expression of GFP. As a result, the P1 cells growing in LB media are larger and brighter than those in M9 minimal media. This observation agrees with the results from flow cytometry measurements obtained in bulk growth experiments, as shown in figure S4.

The transition time from the first steady state before the media exchange to the final steady state in the new media is in the range of 2-3 hours for the P1 strain. It seems that cell dimensions and GFP expression reach their final steady state values at almost the same time. However, the cells start to adjust their length and diameter right after the media shift, while there is a ~40 minute delay before the sharp change of the mean GFP concentration, as shown in figure 2b. This asynchrony may be attributed to the different rates of change of cell volume and GFP expression in the early stage of adaptation. Figure 2b shows that both the cell dimensions and the total amount of GFP per cell decrease right after the media change, which implies that the cells start to shrink their cell sizes and reduce GFP production once they sense the nutritional change. The concomitant change in size and GFP expression in the first hour after downshift results in a constant GFP concentration per cell. Subsequently the concentration of GFP rapidly decreases, indicating a decoupling between gene expression and cell growth as promoter activity is decreased.

Although the fluctuations due to imprecise focusing might reduce the actual temporal resolution of our measurements, we were still able to obtain good reproducibility for the adaptation dynamics between parallel experiments. Figure 3 shows the time-series plots of total fluorescence per cell obtained with the P1 strain from four independent experiments. Despite the notable fluctuation in some curves, we found that all of the curves, either from different fields of view obtained on the same device or for the movies obtained on different days, display a similar trend. The fluorescence increases rapidly after the nutritional upshift and drops after the downshift, with similar rates of change and adaptation time.

Different adaptation dynamics between strains carrying a constitutive promoter and a supercoiling-sensitive promoter

We investigated the adaptive behaviour of two GFP reporter strains. In the first one GFP is expressed under control of a strong, constitutive, promoter from T5 phage (the P5 promoter), and the second one contains a shortened version of a well-studied

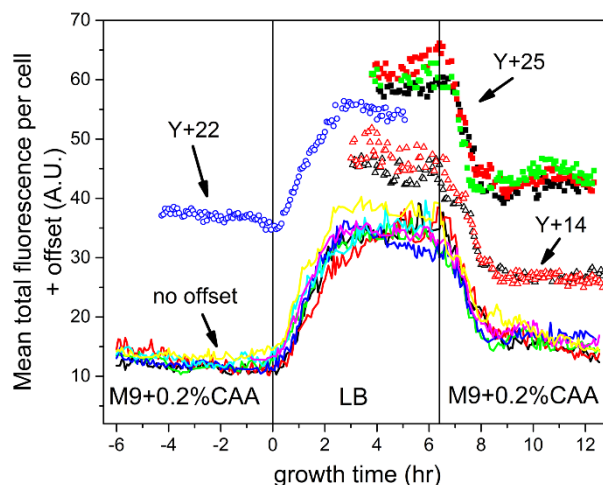


Fig. 3 Reproducibility of the measurements from parallel experiments. The solid lines are obtained from seven fields of view on the same device. The cells first grew in M9 medium with 0.2% CAA for ~10 hours, then in LB medium for ~6 hours and again in M9 medium with 0.2% CAA for another 6 hours. The two vertical lines indicate the two media change time points. The symbols represent the measurements obtained from independent experiments (in different shapes) performed on different devices and on different days, using either an upshift or a downshift. The symbols are plotted with different Y-offset for each experiment but with the same offset for all fields of view (in different colors) in a given experiment. The time points for nutritional upshifts and downshifts in the symbol curves are aligned to the two vertical lines, respectively. Both media contained 50 µg/mL kanamycin and the growth temperature was maintained at 30 °C.

ribosomal RNA promoter *rrnBP1* upstream of the *gfp* gene. The activity of both promoters are expected to increase with the available amount of RNA polymerase, while the activity of *rrnBP1* promoter is also determined by the level of negative supercoiling and the concentration of guanosine pentaphosphate (ppGpp) in the cell³¹. Both strains express the same mutant form of GFP (mut2) [PMID: 8707053]. However, the P1 strain has a higher GFP expression level than the P5 strain. As a result, the P1 cells display brighter fluorescence in both microscopy and flow cytometry experiments.

Figure 4 shows the typical upshift/downshift curves of various cellular parameters for both strains. We do not observe any obvious difference for cell size rearrangement between the two strains or between the nutritional shift directions in figure 4a. This result is expected, as the steady states should be reversible between upshift/downshift and the presence of the GFP promoter should not affect the cell growth. However, the two strains show different adaptive behaviours in GFP expression. The mean total GFP amount per cell of both strains increases with the nutritional upshift and decreases with the nutritional downshift. However, the rates of change (the slopes) for P1 strain are faster than those for the P5 strain, in both the upshift and downshift curves, as seen in figure 4b and figure S5a. This means that the promoter activities in both strains increase with the growth rate, and the promoter activity in P1 cells changes more drastically than that in P5 cells under the same growth conditions. These results are in agreement with those obtained by flow cytometry in an independent experiment using the same strains (Figure S4). The comparison of Supplementary Figure S4 with Figures 3 and 4 also shows the clear superiority in temporal resolution of the

Cite this: DOI: 10.1039/c0xx00000x

www.rsc.org/xxxxxx

ARTICLE TYPE

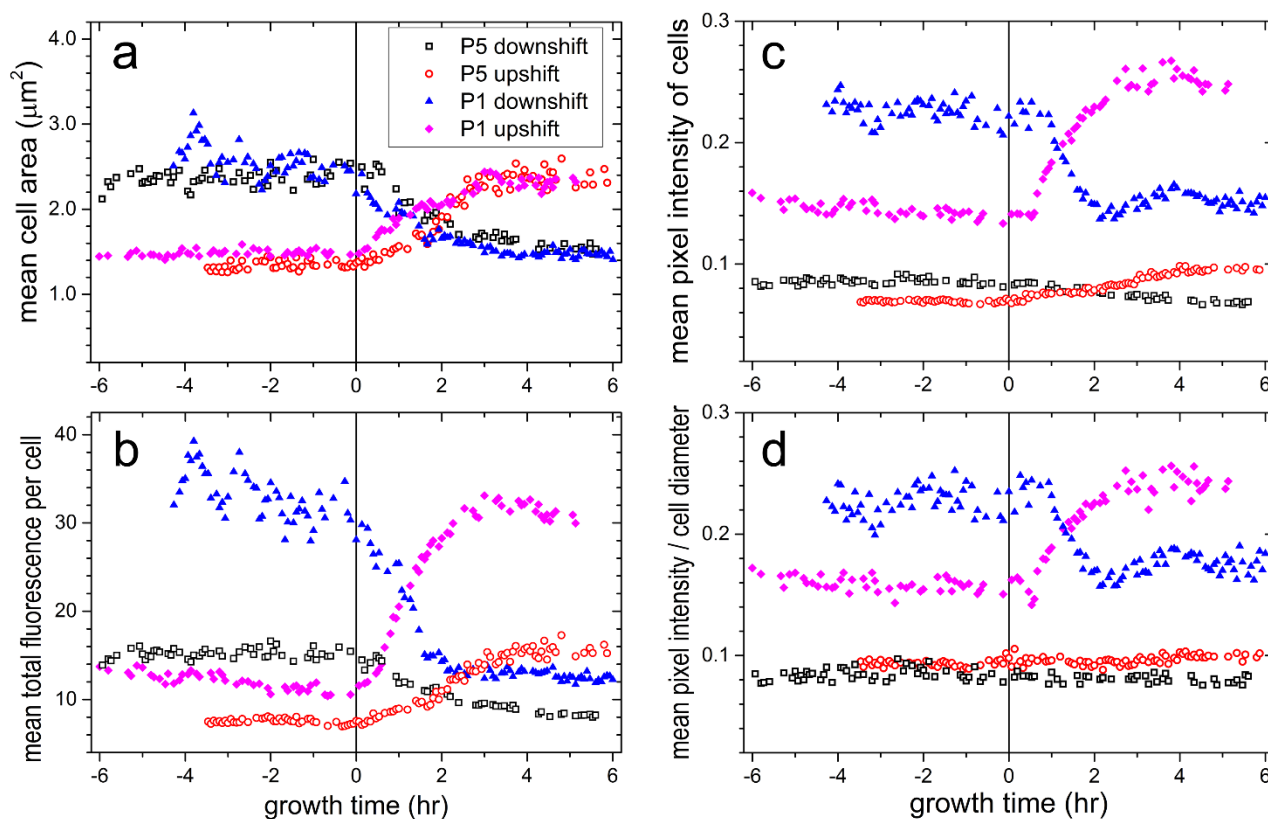


Fig. 4 Time-series plots of mean cell area (a), mean total fluorescence per cell (b), mean pixel intensity of cells (c) and mean GFP concentration (d) measured from typical upshift and downshift movies for cells carrying *rrnB* P1 promoter or P5 promoter. The GFP concentration in cells is estimated by dividing the mean pixel intensity of cells by the mean cell diameter; see the main text for a detailed discussion. The defocused data points have been removed and all the media shift time points are set as zero. The growth conditions are as described in figure 3.

present device. The increased promoter activities result in more GFP production in the cells of both strains during nutritional upshift. Meanwhile, their mean cell volume also increases and causes a dilution effect on intracellular molecules. Consequently, the dynamics of intracellular GFP concentration in an upshift experiment are determined by the balance between the net GFP production rate and the dilution rate caused by the increasing cell volume. Thus, comparing the behaviour of the two different strains is simplest by considering the way the GFP concentration depends on the promoter. Figure 4d and figure S5b show the dynamics of GFP concentration in both strains in the media shift experiments. We observe a sharp increase of mean GFP concentration during nutritional upshift and a decrease during nutritional downshift in P1 cells. This implies that the rate of change of GFP expression in the P1 cells, with the ribosomal RNA promoter construct, is much faster than that of cell volume. There is no significant change in mean GFP concentration for P5 cells during the nutritional upshift or downshift, which indicates that the dilution/concentration effects by the cell size rearrangement balances the increase/decrease of GFP production in P5 cells with a constitutive promoter.

Other researchers had observed a decrease in protein concentration at faster growth in some reporter strains containing different constitutive promoters from the one used here^{37, 40}. This difference is likely due to the fact that a constitutive promoter is a general term that refers to a promoter that is not under any specific regulation from transcription factors. However, the difference in affinity of the specific promoter for RNA polymerase can result in a different level of expression and thus more or less dilution by the change in growth rate. Both promoters contain the -35 and -10 consensus sequences resulting in a high affinity for RNA polymerase and should thus respond to the increased amount of RNA polymerase⁴¹ in a similar way. We thus attribute the different adaptive behaviour in GFP expression of the P1 strain to the particular dependency of its promoter activity on the level of negative supercoiling and on the concentration of guanosine pentaphosphate (ppGpp) in cell.

Conclusions

We quantitatively compared the single-cell adaptive behaviors of two engineered *E. coli* strains during nutritional upshift or

downshift using a microfluidic chemostat and time-lapse fluorescence microscopy. We found that both the cell dimensions and the total GFP amount per cell in both strains increase when the growth medium is changed from nutrient-poor media to nutrient-rich media, and vice versa. There is no obvious difference of adaptation dynamics between the two strains for cell size rearrangement. However, the GFP expression dynamics of these two strains are distinctly different; the P1 cells carrying a ribosomal RNA promoter have a faster GFP production rate than the dilution/concentration rate by the changing cell volume; the latter however plays a more important role in P5 cells with a constitutive promoter. As a result, the GFP concentration in P1 cells changes rapidly during nutritional upshift or downshift and this change in P5 cells is very small.

We demonstrate that we can simultaneously measure the dynamics of various cell dimensions, the total GFP amount and the GFP concentrations in individual bacterial cells from the fluorescence microscopy images with high temporal resolution. The total amount of GFP per cell can also be measured by flow cytometry with better accuracy but lower temporal resolution, and it is very difficult to obtain precise cell dimensions for the small bacterial cells by light scattering in a regular flow cytometer. Flow cytometry thus cannot provide the dynamic information of the intracellular protein concentrations in single cells, which is very important in understanding and modeling the regulation mechanism of gene networks in bacteria.

The microfluidic chemostat offers faster media change and much longer observation time than conventional agar-based devices. Although the actual temporal resolution in this study was affected by imprecise autofocusing, we anticipate that we will be able to measure the adaptation dynamics of *E. coli* cells with higher resolution and accuracy by incorporating hardware-based autofocusing into our microscope and imaging from more fields of view. These improvements, which involve off-the-shelf components, will allow us to carry out experiments in more reporter strains and under more growth conditions in order to identify the cellular mechanisms determining the timing of gene expression change.

This study, together with our previous work²⁴, suggest that the present microfluidic chemostat is a versatile platform for measuring single-cell dynamics of various cellular parameters in bacteria, either in balanced growth or in dynamical environments.

Acknowledgements

This work was supported by the HFSP grant RGY0069/2009-C and a Teacher-Scholar Award from the Camille and Henry Dreyfus Foundation to KDD. Portions of this work were performed in the University of Minnesota Nano Center, which receives partial support from the NSF through the National Nanotechnology Infrastructure Network (NNIN).

Notes and references

^a Department of Chemical Engineering and Materials Science, University of Minnesota - Twin Cities, 421

Washington Ave. SE, Minneapolis, MN 55455, USA. E-mail: dorfman@umn.edu

^b LBPA, UMR 8113 du CNRS, Ecole Normale Supérieure de Cachan, France

^c Sorbonne Universités, UPMC Univ Paris 06, UMR 7238, Computational and Quantitative Biology, 15 rue de l'

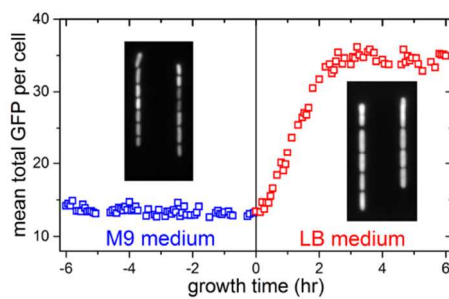
^d École de Médecine Paris, F-75006 France

^e CNRS, UMR 7238, Paris, France

† Electronic Supplementary Information (ESI) available: [Supplementary movie S1 and S2, figures S1-S5]. See DOI: 10.1039/b000000x/

- H. Rediers, P. B. Rainey, J. Vanderleyden and R. De Mot, *Microbiol. Mol. Biol. Rev.*, 2005, **69**, 217-261.
- I. Cases, V. de Lorenzo and C. A. Ouzounis, *Trends Microbiol.*, 2003, **11**, 248-253.
- S. Jozefczuk, S. Klie, G. Catchpole, J. Szymanski, A. Cuadros-Inostroza, D. Steinhäuser, J. Selbig and L. Willmitzer, *Mol. Syst. Biol.*, 2010, **6**, 364.
- M. Y. Pavlov and M. Ehrenberg, *Proc. Natl. Acad. Sci. U. S. A.*, 2013, **110**, 20527-20532.
- D. Longo and J. Hasty, *Mol. Syst. Biol.*, 2006, **2**, 64.
- B. F. Brehm-Stecher and E. A. Johnson, *Microbiol. Mol. Biol. Rev.*, 2004, **68**, 538-559.
- D. R. Larson, R. H. Singer and D. Zenklusen, *Trends Cell Biol.*, 2009, **19**, 630-637.
- B. P. Tracy, S. M. Gaida and E. T. Papoutsakis, *Curr. Opin. Biotechnol.*, 2010, **21**, 85-99.
- S. Muller, T. Bley and W. Babel, *J. Biotechnol.*, 1999, **75**, 81-97.
- T. S. Hawley, D. J. Herbert, S. S. Eaker and R. G. Hawley, *Methods Mol. Biol.*, 2004, **263**, 219-238.
- I. A. Zuleta, A. Aranda-Diaz, H. Li and H. El-Samad, *Nat. methods*, 2014, **11**, 443-448.
- O. Julia, J. Comas and J. Vives-Rego, *J. Microbiol. Methods*, 2000, **40**, 57-61.
- Y. Wakamoto, N. Dhar, R. Chait, K. Schneider, F. Signorino-Gelo, S. Leibler and J. D. McKinney, *Science*, 2013, **339**, 91-95.
- S. G. Megason and S. E. Fraser, *Cell*, 2007, **130**, 784-795.
- J. W. Young, J. C. W. Locke, A. Altinok, N. Rosenfeld, T. Bacarian, P. S. Swain, E. Mjolsness and M. B. Elowitz, *Nat. Protoc.*, 2012, **7**, 80-88.
- J. A. Megerle, G. Fritz, U. Gerland, K. Jung and J. O. Radler, *Biophys. J.*, 2008, **95**, 2103-2115.
- P. Meyer and J. Dworkin, *Res. Microbiol.*, 2007, **158**, 187-194.
- W. Mather, O. Mondragon-Palomino, T. Danino, J. Hasty and L. S. Tsimring, *Phys. Rev. Lett.*, 2010, **104**, 208101.
- A. Grunberger, N. Paczia, C. Probst, G. Schendzielorz, L. Eggeling, S. Noack, W. Wiechert and D. Kohlheyer, *Lab Chip*, 2012, **12**, 2060-2068.
- G. Ullman, M. Wallden, E. G. Marklund, A. Mahmutovic, I. Razinkov and J. Elf, *Philos. Trans. R. Soc. B*, 2013, **368**, 20120025.
- I. Wong, S. Atsumi, W.-C. Huang, T.-Y. Wu, T. Hanai, M.-L. Lam, P. Tang, J. Yang, J. C. Liao and C.-M. Ho, *Lab Chip*, 2010, **10**, 2710-2719.
- S. Boulineau, F. Tostevin, D. J. Kiviet, P. R. ten Wolde, P. Nghe and S. J. Tans, *PLoS One*, 2013, **8**, e61686.
- J. B. Nobs and S. J. Maerkl, *PLoS One*, 2014, **9**, e93466.
- Z. Long, E. Nugent, A. Javer, P. Cicuta, B. Sclavi, M. C. Lagomarsino and K. D. Dorfman, *Lab Chip*, 2013, **13**, 947-954.
- P. Wang, L. Robert, J. Pelletier, W. L. Dang, F. Taddei, A. Wright and S. Jun, *Curr. Biol.*, 2010, **20**, 1099-1103.
- J. R. Moffitt, J. B. Lee and P. Cluzel, *Lab Chip*, 2012, **12**, 1487-1494.
- C. Probst, A. Grunberger, W. Wiechert and D. Kohlheyer, *Micromachines*, 2013, **4**, 357-369.
- A. Javer, Z. C. Long, E. Nugent, M. Grisi, K. Siriawetchakul, K. D. Dorfman, P. Cicuta and M. C. Lagomarsino, *Nat. Commun.*, 2013, **4**, 3003.
- A. Javer, N. J. Kuwada, Z. Long, V. G. Benza, K. D. Dorfman, P. A. Wiggins, P. Cicuta and M. C. Lagomarsino, *Nat. Commun.*, 2014, **5**, 3854.
- K. A. Datsenko and B. L. Wanner, *Proc. Natl. Acad. Sci. U. S. A.*, 2000, **97**, 6640-6645.
- M. S. Bartlett and R. L. Gourse, *J. Bacteriol.*, 1994, **176**, 5560-5564.
- A. Edelstein, N. Amodaj, K. Hoover, R. Vale and N. Stuurman, *Curr. Protoc. Mol. Biol.*, 2010, 14.20.11 - 14.20.17.
- A. E. Carpenter, T. R. Jones, M. R. Lamprecht, C. Clarke, I. H. Kang, O. Friman, D. A. Guertin, J. H. Chang, R. A. Lindquist, J. Moffat, P. Golland and D. M. Sabatini, *Genome Biol.*, 2006, **7**, R100.
- J. C. W. Locke and M. B. Elowitz, *Nat. Rev. Microbiol.*, 2009, **7**, 383-392.

-
- 1 35. A. C. Chien, N. S. Hill and P. A. Levin, *Curr. Biol.*, 2012, **22**, R340-
2 R349.
- 3 36. M. Schaechter, O. Maaloe and N. O. Kjeldgaard, *J. Gen. Microbiol.*,
4 1958, **19**, 592-606.
- 5 37. S. Klumpp and T. Hwa, *Curr. Opin. Biotechnol.*, 2014, **28C**, 96-102.
- 6 38. F. J. Trueba and C. L. Woldringh, *J. Bacteriol.*, 1980, **142**, 869-878.
- 7 39. A. Zaritsky, C. L. Woldringh, C. E. Helmstetter and N. B. Grover, *J.*
8 *Gen. Microbiol.*, 1993, **139**, 2711-2714.
- 9 40. S. Klumpp, Z. G. Zhang and T. Hwa, *Cell*, 2009, **139**, 1366-1375.
- 10 41. S. Klumpp and T. Hwa, *Proc. Natl. Acad. Sci. U. S. A.*, 2008, **105**,
11 20245-20250.
- 12
- 13
- 14
- 15
- 16
- 17
- 18
- 19
- 20
- 21
- 22
- 23
- 24
- 25
- 26
- 27
- 28
- 29
- 30
- 31
- 32
- 33
- 34
- 35
- 36
- 37
- 38
- 39
- 40
- 41
- 42
- 43
- 44
- 45
- 46
- 47
- 48
- 49
- 50
- 51
- 52
- 53
- 54
- 55
- 56
- 57
- 58
- 59
- 60



We grew *E. coli* in a microfluidic chemostat and monitored the dynamics of cell dimensions and reporter GFP expression in individual cells during nutritional upshift or downshift.